Acta Crystallographica Section B
Structural Science
ISSN 0108-7681

Neutron powder diffraction study of orthorhombic and monoclinic defective silicalite

G. Artioli,[a]* C. Lamberti[b] and G. L. Marra[c]

[a]Dipartimento di Scienze della Terra, Università di Milano, via Botticelli 23, I-20133 Milano, Italy, [b]Dipartimento di Chimica Inorganica, Chimica Fisica e Chimica dei Materiali, Università di Torino, via P. Giuria 7, I-10125 Torino, Italy, and [c]Enichem s.p.a., Centro Ricerche Novara, Istituto G. Donegani, via G. Fauser 4, I-28100 Novara, Italy

Correspondence e-mail: artioli@iummix.terra.unimi.it

Received 6 May 1999
Accepted 30 June 1999

The crystal structure of silicalite (SiO_2) with a substantial amount of structural hydroxyl groups [$Si_{(1-x)}O_{(2-4x)}(OH)_{4x}$, with $0.08 < x < 0.10$] has been refined from neutron powder diffraction data measured using the HRPD instrument at the ISIS pulsed neutron source. Powder data were collected on the as-synthesized orthorhombic sample at 298 K, and on the deuterated monoclinic sample at 100 K. Preferential location of Si-atom vacancies was found on four out of 12 independent *T* sites in the orthorhombic silicalite [Si(6), Si(7), Si(10) and Si(11)], although the H atoms of the substituting hydroxyl groups could not be located because of the low statistical site occupancy on multiple sites. No significant population of D atoms or of Si vacancies was found in the tetrahedral sites of the monoclinic sample. The detected long-range order of adjacent Si atoms in defective orthorhombic [MFI] structures is compatible with a mechanism of Si vacancy clustering and with the model of hydroxyl nests assumed in the literature on the basis of IR spectroscopic evidence. Crystal data: orthorhombic, *Pnma*, $Z = 8$, $a = 20.0511\ (1)$, $b = 19.8757\ (1)$, $c = 13.36823\ (9)$ Å, $V = 5327.62\ (5)$ Å^3, $D_x = 1.798$ g cm^{-3}, $M_r = 721.01$; monoclinic, $P2_1/n$, $Z = 4$, $a = 19.8352\ (2)$, $b = 20.0903\ (2)$, $c = 13.3588\ (1)$ Å, $\beta = 90.892\ (1)^\circ$, $V = 5322.78\ (6)$ Å^3, $D_x = 1.799$ g cm^{-3}, $M_r = 1442.02$.

1. Introduction

Silicalite, synthesized first by the Union Carbide group (Flaningen *et al.*, 1978), is an aluminium-free zeolite, belonging to the structure type MFI in the IUPAC nomenclature (Szostak, 1989; Meier *et al.*, 1996). It shows a three-dimensional pore system consisting of two intersecting sets of tubular channels: a linear one parallel to the [010] direction having openings of 5.4 × 5.6 Å, and a sinusoidal one parallel to the [100] direction with openings of 5.1 × 5.5 Å (Kokotailo *et al.*, 1978; Olson *et al.*, 1981). Both channels are defined by ten-membered rings of SiO_4 tetrahedra.

Its discovery has opened the possibility of creating a great number of new microporous materials. Besides the interest from a crystallographic and mineralogical point of view (a recently discovered natural zeolite, mutinaite, has the MFI topology; Vezzalini *et al.*, 1997), the MFI-type materials have shown a tremendous impact as new shape-selective industrial catalysts having tunable acidic strength. In fact, the isomorphous substitution of Si by other tetrahedrally coordinated elements such as B^{III} (Coudurier *et al.*, 1987), Al^{III} (ZSM-5; Kokotailo *et al.*, 1978), Ti^{IV} (Ti-silicalite or TS-1; Bordiga, Coluccia *et al.*, 1994; Taramasso *et al.*, 1983; Scarano *et al.*, 1993; Tozzola *et al.*, 1998; Zecchina *et al.*, 1996), Fe^{III} (Bordiga *et al.*, 1996; Geobaldo *et al.*, 1996; Szostak & Thomas, 1986)

and Ga^{III} (Otero Areán *et al.*, 1996; Bayese *et al.*, 1992; Liu & Klinowski, 1992) in a small amount (1–3 wt%) provides new materials showing specific catalytic properties in oxidation and hydroxylation reactions related to the coordination state of the heteroatom. Moreover, when trivalent metals are present in *T* sites, the zeolite framework has a net negative charge which can be balanced by a number of bridged $Si(OH)M^{III}$ protons (M = B, Al, Fe, Ga), effectively yielding microporous solids with Brønsted acidity. Since the acidic strength of the OH group depends upon the nature of the trivalent heteroatom, the choice of M^{III} critically affects the acidic strength of the zeolite material (Al > Fe ∼ Ga >> B; Chu & Chang, 1985).

Silicalite itself exhibits a very low acidic behaviour and it has a proven selective ability to catalyze reactions occurring only under very mild conditions, preventing the formation of undesired side products (such as the coking process). The nature of the low acidic property of silicalite is attributed to the presence of internal defects: the lack of one or more adjacent Si atoms is balanced by the presence of hydroxylated nano-cavities in the framework, also referred to as hydroxyl nests (Zecchina, Bordiga, Spoto, Marchese, Petrini, Leofanti & Padovan, 1992; Zecchina, Bordiga, Spoto, Scarano *et al.*, 1992; Zecchina, Bordiga, Spoto, Marchese, Petrini, Leofanti, Padovan & Otero Areàn, 1992; Marra *et al.*, 1994), as shown in Fig. 1. In this respect, silicalites synthesized following the EniChem patent for TS-1 (Taramasso *et al.*, 1983) in the absence of TiO_2 show a much lower level of Na, Al impurity species and a higher OH defect density (Marra *et al.*, 1994; Zecchina, Bordiga, Spoto, Marchese, Petrini, Leofanti & Padovan, 1992; Zecchina, Bordiga, Spoto, Scarano *et al.*, 1992; Zecchina, Bordiga, Spoto, Marchese, Petrini, Leofanti, Padovan & Otero Areàn, 1992) than silicalites synthesized following the original patent (Flaningen *et al.*, 1978). The absence of impurities and the presence of internal hydroxyl nests has consequences on the long-range structural order, since the calcined samples show orthorhombic symmetry if prepared as described by Zecchina, Bordiga, Spoto, Marchese, Petrini, Leofanti & Padovan (1992) and monoclinic symmetry if prepared following the original recipe (Flaningen *et al.*, 1978). Moreover, the two products show remarkable differences in the crystal size, the former yielding a high-surface-area powder with grains in the 220–260 nm range, whereas the latter has grains in the 2000–3500 nm interval, as determined by high-resolution transmission electron microscopy (Zecchina, Bordiga, Spoto, Scarano *et al.*, 1992).

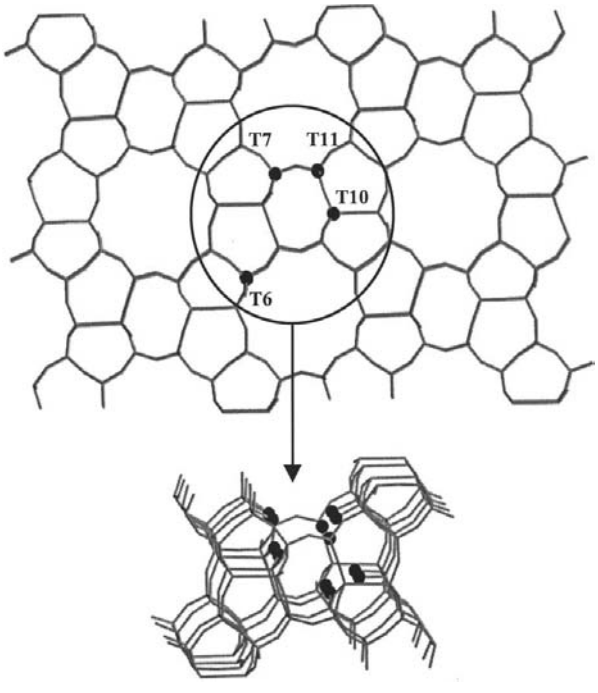

Figure 1
Top: view of a defect-free MFI framework along the [010] direction. The *T*6, *T*7, *T*10 and *T*11 positions are shown as black circles. Bottom: enlargement of the circled area of (*a*) where six adjacent *T*7, *T*10 and *T*11 sites have been omitted, showing one of the theoretical configurations of vacancy nests. The black spheres are the O atoms corresponding to the 12 OH groups of the hydroxyl nest.

The detailed crystal structural and chemical role of OH groups in silicalite is still debated, although it is known that their presence dramatically improves the framework interaction with guest molecules and increases the absorption capacity. The interest of defective silicalites in catalysis is due to the presence of internal silanol groups. Models for the location and clustering of the hydroxyl groups in silicalite have been proposed on the basis of spectroscopic (IR) and volumetric observations complemented by molecular dynamics simulations (Zecchina, Bordiga, Spoto, Marchese, Petrini, Leofanti & Padovan, 1992; Zecchina, Bordiga, Spoto, Scarano *et al.*, 1992; Zecchina, Bordiga, Spoto, Marchese, Petrini, Leofanti, Padovan & Otero Areàn, 1992; Bordiga, Ricchiardi *et al.*, 1994; Marra *et al.*, 1994). These studies have provided evidence that the presence of isolated Si vacancies alone is not able to explain the increased adsorption capabilities of this silicalite and the lack of two or more adjacent *T* sites must be assumed. The IR experimental evidence indicates that internal OH have a slightly higher acidity compared with external silanols and that a considerable fraction of protons are involved in weak hydrogen bonds, resulting in the formation of hydroxyl nests.

In the present study the long-range ordering of such internal defects is investigated to check whether the Si atom vacancies occur randomly over the crystallographically independent tetrahedral sites of the MFI framework, or whether there are preferential defective tetrahedral sites. The issue has implications in the structural interpretation of the nature of the low-strength acidic sites in these important catalyst materials, especially because metal-substituted silicalites also show a certain degree of *M*OH defects (M = Al, Ti, Fe, Ga), as observed on ZSM-5 (Vedrine *et al.*, 1979; Dessau *et al.*, 1987; Hunger *et al.*, 1987; Zecchina, Bordiga, Spoto, Marchese, Petrini, Leofanti, Padovan & Otero Areàn, 1992), on TS-1 (Zecchina *et al.*, 1991; Lamberti *et al.*, 1998; Bolis *et al.*, 1999*a*,*b*; Le Noc *et al.*, 1996), on Fe-silicalite (Geobaldo *et al.*, 1996) and Ga-silicalite (Bayese *et al.*, 1992; Liu & Klinowski, 1992). In the cited works the presence of a significant amount

Table 1
Data collection and Rietveld refinement parameters.

	ORTHO	MONO
Accumulation time (h)	24	24
T (K)	298	100
TOF range (ms) – 168° bank	48–130	48–130
TOF range (ms) – 90° bank	48–135	48–135
a (Å)	20.0511 (1)	19.8352 (2)
b (Å)	19.8757 (1)	20.0903 (2)
c (Å)	13.36823 (9)	13.3588 (1)
β (°)		90.892 (1)
Space group	*Pnma*	$P2_1/n$
wRp	0.0333	0.0247
Rp	0.0310	0.0293
χ^2	3.08	1.95
Total no. of experimental points	19 301	20 483

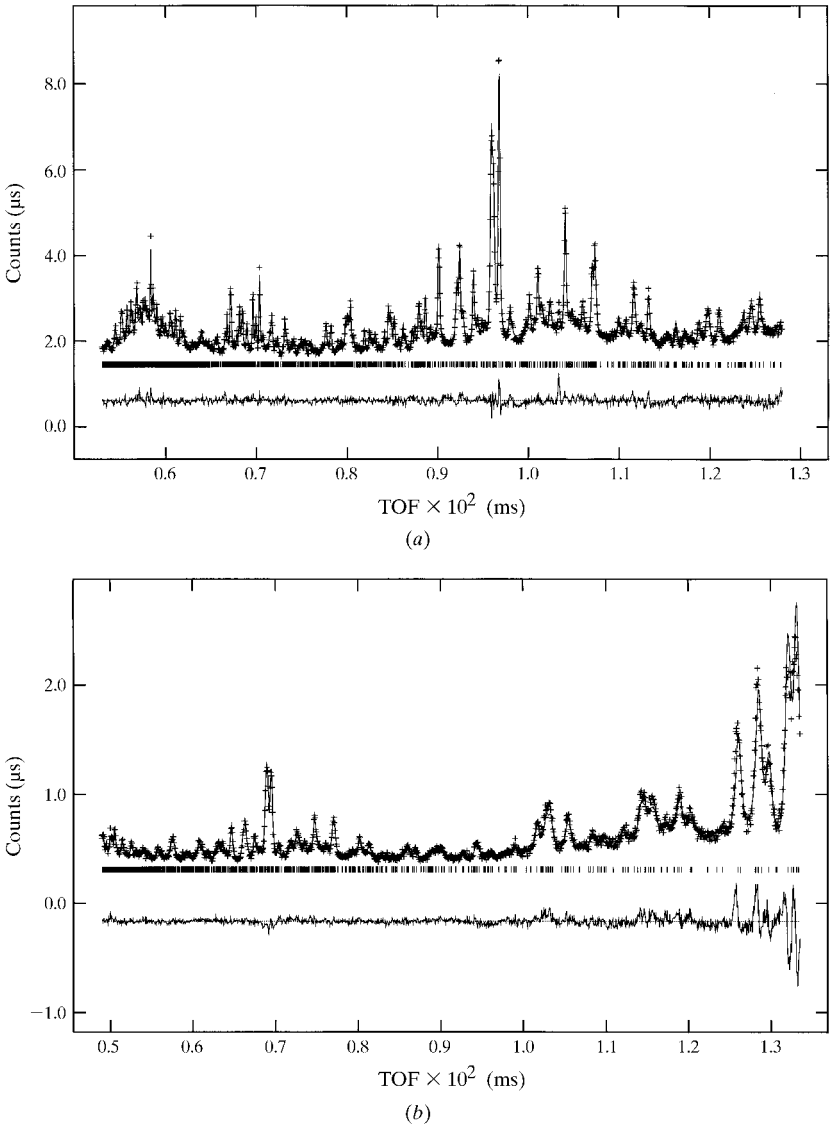

Figure 2
Final observed (crosses), calculated (solid upper line) and difference (solid lower line) powder diffraction patterns for orthorhombic silicalite (ORTHO sample). (*a*) Data from the HRPD detector bank at 168°. (*b*) Data from the HRPD detector bank at 90°.

of *T*-atom vacancies and the related presence of internal *T*OH hydroxyls (*T* = Si, Al, Ti, Fe, Ga) has been experimentally proven by IR, NMR, microcalorimetry and EXAFS.

From the crystallographic point of view all synthetic MFI zeolites show a polymorphic orthorhombic-to-monoclinic phase transition. The transition temperature and mechanism is closely related to the composition and defect density of the tetrahedral framework, besides of course the nature and amount of the molecules absorbed in the zeolitic channels. At room temperature the as-synthesized samples of hydrogen-free ZSM-5 and TS-1 are orthorhombic *Pnma*, whereas hydrogen-containing ZSM-5 (Van Koningsveld *et al.*, 1990) and TS-1 with very low Ti content (Millini *et al.*, 1992, 1999; Lamberti *et al.*, 1999) are monoclinic $P2_1/n$. The pure silicalite end-member at room temperature is monoclinic $P2_1/n$ and reversibly transforms to orthorhombic at high temperature. The orthorhombic form can also be stabilized by insertion of an adequate amount of structural defects (Marra *et al.*, 1994) or by absorption of various molecules in the channels (benzene, paraxylene *etc.*). The defect-stabilized orthorhombic polymorph readily re-transforms to monoclinic upon water treatment.

In the present study we synthesized a sample of orthorhombic silicalite $Si_{(1-x)}O_{(2-4x)}(OH)_{4x}$ with a high content of structural hydroxyls ($0.08 < x < 0.10$) and refined the structure by neutron powder diffraction data in order to gain evidence for the possible segregation of the defects in some of the 12 crystallographically independent tetrahedral sites. Since H in the naturally occurring isotopic proportions has a large incoherent scattering, and diffraction data of hydrogen-containing samples contain a substantial level of non-Bragg scattering contributing to the experimental background, the defect-loaded silicalite sample was also deuterated in order to improve the diffraction signal. As discussed, the sample treatment with D_2O invariably induces the orthorhombic-to-monoclinic transition, and the amount of OD defects present in the structure after complete deuteration is unknown. Two samples were therefore used for data collection: one orthorhombic as-synthesized sample (ORTHO) and one monoclinic sample which underwent complete deuteration (MONO).

2. Experimental

The silicalite sample was synthesized starting from SiO_2 sol using TPAOH as a templating agent as described by Zecchina, Bordiga, Spoto, Marchese, Petrini, Leofanti & Padovan (1992), *i.e.* following the EniChem patent for TS-1 (Taramasso *et al.*, 1983) with no addition

of TiO_2. The sample was then calcined at 823 K for organic template removal and sealed in a glass vial to avoid water sorption from the atmosphere: this procedure ensures that no molecules are present in the zeolitic channels. The as-calcined silicalite (hereafter labelled as the ORTHO sample) showed orthorhombic symmetry, in agreement with previous results (Zecchina, Bordiga, Spoto, Scarano *et al.*, 1992; Marra *et al.*, 1994). The defect density in the sample was evaluated by chemical analysis and volumetric measurements. Part of the ORTHO sample was repeatedly soaked in D_2O at 423 K for H $\rightarrow$ D exchange. After this treatment the deuterated silicalite (hereafter indicated as the MONO sample) has undergone the orthorhombic monoclinic transition. The deuteration process was followed by a shift of the IR absorption peaks characteristic of the OH (DH) stretching modes. The fully deuterated MONO sample was then dehydrated in a vacuum at 773 K and then sealed in a glass vial. The vial was kept in deuterated water until the time of the experiment to avoid rehydrogenation of the sample, and data were collected at 100 K in order to minimize atomic thermal vibrations and increase the chances of locating the D atoms. The data of the ORTHO sample were collected at room temperature because the addition of the instrumental background from the cryostat to the intrinsic background of the hydrogen-rich sample made the signal-to-noise ratio in the powder diffraction patterns insufficient for a successful structure analysis.

For each sample approximately 3 cm^3 of silicalite was loaded into the glass sample holder. Data were collected on the HRPD instrument at ISIS (Didcot, UK) for 24 h in order to obtain high-quality statistics. Two ZnS scintillator banks at 168° and 90° with respect to the incident beam were used. The HRPD instrument is well suited for investigation of complex low-symmetry materials, since at backscattering it offers a very high resolution ($\Delta d/d \simeq 4$–5×10^{-4}), almost constant through the diffraction pattern. The data from the 90° bank were used in the time-of-flight range 48–135 ms (corresponding to the range 1.38–3.90 Å in d-space) and those from the 168° bank in the time-of-flight range 48–130 ms (0.99–2.70 Å in d-space). The two independently measured powder patterns for each sample were simultaneously used in the structural Rietveld refinement.

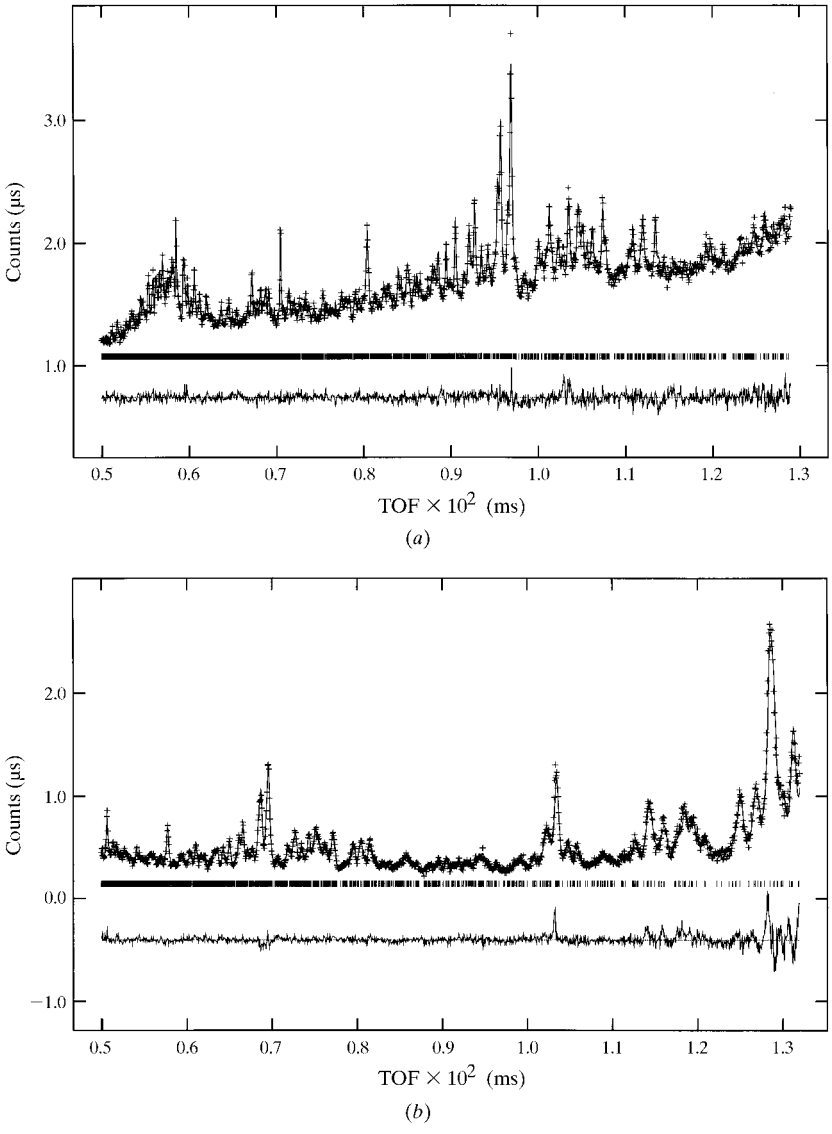

Figure 3
Final observed (crosses), calculated (solid upper line) and difference (solid lower line) powder diffraction patterns for monoclinic silicalite (MONO sample). (*a*) Data from the HRPD detector bank at 168°. (*b*) Data from the HRPD detector bank at 90°.

Detector calibration, source-to-sample distance and starting peak profile parameters were obtained by careful refinement of the powder diffraction data of reference BaF_2 collected under the same experimental conditions. The Rietveld analysis was performed using the *GSAS* program package (Larson & Von Dreele, 1998). The peak profiles were modelled by a convolution of a double-exponential and a switch function (Ikeda & Carpenter, 1985) with a pseudo-Voigt function; the Lorentzian breadth of the peak FWHM is parametrized as $\gamma = \gamma_0 + \gamma_1 d_{hkl} + \gamma_2 d_{hkl}^2$ and the Gaussian breadth as $\sigma = \sigma_0 + \sigma_1 d_{hkl}^2 + \sigma_2 d_{hkl}^4$. Given the large number of structural parameters, the refinement was started by imposing severe constraints on the T—O bond distances. The weights of the constraints were progressively released at convergence. Furthermore, the isotropic atomic displacement parameters (a.d.p.s) of all Si and O sites were constrained to be equal, thus limiting the number of refined a.d.p.s to two. The instrumental background was modelled by a Chebyschev polynomial with six refinable coefficients. In the final cycles all atomic coordinates, two isotropic a.d.p.s, one scale factor and two peak profile coefficients (σ_1 and γ_2) for each histogram, the cell parameters, and six

Table 2
Refined atomic coordinates of orthorhombic H silicalite (ORTHO sample).

$$U_{eq} = (1/3)\Sigma_i\Sigma_j U^{ij} a^i a^j \mathbf{a}_i.\mathbf{a}_j.$$

The final refinement was performed with full occupancy on all Si and O atoms (see text for details). The average Si—O tetrahedral distances (Å) are reported for the *T* sites, and the Si—O—Si angles (°) are reported for the O sites.

	x	*y*	*z*	Mean Si—O distance	U_{eq}
Si(1)	0.4245 (3)	0.0601 (3)	−0.3315 (4)	1.600 (2)	0.0256 (4)
Si(2)	0.3083 (3)	−0.0281 (2)	−0.1860 (4)	1.601 (2)	0.0256 (4)
Si(3)	0.2779 (3)	0.0612 (3)	0.0341 (4)	1.603 (2)	0.0256 (4)
Si(4)	0.1182 (3)	0.0628 (3)	0.0283 (4)	1.600 (2)	0.0256 (4)
Si(5)	0.0749 (3)	0.0289 (3)	−0.1874 (5)	1.601 (2)	0.0256 (4)
Si(6)	0.1888 (3)	−0.0607 (3)	−0.3272 (4)	1.600 (2)	0.0256 (4)
Si(7)	0.4249 (3)	−0.1723 (2)	−0.3265 (4)	1.602 (2)	0.0256 (4)
Si(8)	0.3087 (3)	−0.1321 (3)	−0.1842 (4)	1.599 (2)	0.0256 (4)
Si(9)	0.2721 (3)	−0.1754 (2)	0.0335 (4)	1.603 (2)	0.0256 (4)
Si(10)	0.1199 (3)	−0.1738 (2)	0.0320 (4)	1.602 (2)	0.0256 (4)
Si(11)	0.0723 (3)	−0.1292 (3)	−0.1809 (5)	1.601 (2)	0.0256 (4)
Si(12)	0.1858 (3)	−0.1732 (2)	−0.3233 (4)	1.600 (2)	0.0256 (4)

	x	*y*	*z*	Si—O—Si angle	U_{eq}
O(1)	0.3777 (3)	0.0495 (5)	−0.2359 (5)	151.4 (6)	0.0408 (4)
O(2)	0.3060 (5)	0.0631 (4)	−0.0782 (4)	147.4 (6)	0.0408 (4)
O(3)	0.1981 (3)	0.0601 (4)	0.0274 (4)	175.4 (5)	0.0408 (4)
O(4)	0.0989 (3)	0.0663 (4)	−0.0876 (4)	149.3 (6)	0.0408 (4)
O(5)	0.1161 (3)	0.0616 (5)	−0.2776 (5)	141.1 (5)	0.0408 (4)
O(6)	0.2487 (3)	0.0618 (5)	−0.2482 (5)	153.8 (7)	0.0408 (4)
O(7)	0.3745 (4)	−0.1628 (4)	−0.2343 (6)	152.3 (7)	0.0408 (4)
O(8)	0.3077 (5)	−0.1545 (3)	−0.0694 (4)	154.2 (7)	0.0408 (4)
O(9)	0.1963 (3)	−0.1505 (3)	0.0227 (5)	143.8 (4)	0.0408 (4)
O(10)	0.0876 (4)	−0.1665 (4)	−0.0772 (5)	155.1 (6)	0.0408 (4)
O(11)	0.1152 (3)	−0.1546 (4)	−0.2746 (6)	150.0 (7)	0.0408 (4)
O(12)	0.2437 (4)	−0.1531 (4)	−0.2462 (6)	171.2 (8)	0.0408 (4)
O(13)	0.3153 (4)	−0.0521 (2)	−0.1876 (4)	169.9 (6)	0.0408 (4)
O(14)	0.0840 (3)	−0.0501 (3)	−0.1678 (5)	158.2 (5)	0.0408 (4)
O(15)	0.4193 (4)	0.1321 (4)	−0.3842 (6)	143.5 (6)	0.0408 (4)
O(16)	0.4054 (4)	0.0006 (4)	−0.4069 (6)	173.4 (7)	0.0408 (4)
O(17)	0.4014 (4)	−0.1346 (4)	−0.4264 (6)	143.6 (6)	0.0408 (4)
O(18)	0.1906 (5)	0.1319 (3)	−0.3828 (5)	144.5 (7)	0.0408 (4)
O(19)	0.1899 (5)	0.0019 (3)	−0.4089 (5)	154.3 (7)	0.0408 (4)
O(20)	0.1959 (6)	−0.1323 (3)	−0.4251 (4)	141.3 (6)	0.0408 (4)
O(21)	−0.0021 (3)	0.0441 (4)	−0.2093 (5)	149.5 (6)	0.0408 (4)
O(22)	−0.0019 (3)	−0.1513 (5)	−0.2103 (6)	148.0 (5)	0.0408 (4)
O(23)	0.4287 (7)	−1/4	−0.3573 (9)	149.6 (9)	0.0408 (4)
O(24)	0.2025 (6)	−1/4	−0.3473 (8)	146.2 (8)	0.0408 (4)
O(25)	0.2881 (6)	−1/4	0.0722 (7)	135.3 (8)	0.0408 (4)
O(26)	0.1136 (7)	−1/4	0.0696 (9)	142.2 (9)	0.0408 (4)

coefficients of the background modelling function were simultaneously refined. Detailed strategies of the refinement of site occupancy factors are discussed below.

Table 1 reports the details of the data collection and Rietveld refinements.[1] Figs. 2 and 3 show the observed, calculated and difference powder diffraction spectra for the final refinements of the ORTHO and MONO silicalite samples, respectively. Primary powder diffraction data have been deposited at the International Centre for Diffraction Data (ICDD), 12 Campus Boulevard, Newton Square, PA 19073–3273, USA. Final position and isotropic thermal parameters of the ORTHO and MONO structures are reported in Tables 2 and 3, together with the mean tetrahedral distances and *T*—O—*T* angles. The full list of interatomic distances and angles is available from the authors upon request.

3. Refinement of the *T* site occupancies and discussion

The strategy of the structure refinement focused on the detection of possible *T* centres showing an Si occupancy significantly smaller than unity, which of course is related to the insertion of neighbouring H (or D) atoms of the adjacent hydroxyls formed upon silicon elimination. It is evident that high-resolution neutron diffraction is the technique of choice to investigate such a problem, both because of its ability to detect protons (deuterons in particular) and because of the low achievable *d*-spacing value.

The structural models of orthorhombic and monoclinic silicalite present in the literature (Van Koningsveld *et al.*, 1987, 1990) were used as starting models for the Rietveld refinement. The results of the idealized model with full occupancy of all tetrahedral sites are reported in Tables 2 and 3. The residual difference Fourier maps were carefully inspected for positive (MONO sample) or negative (ORTHO sample) peaks within the tetrahedra or close to the framework O atoms. For both samples no significant peak was detected above the map background noise or distinguishable from the ripples due to the isotropic displacement approximation employed to model the framework atoms. Some residual small peaks of difficult interpretation, at distances of ∼1.0 Å from O atoms, were tentatively interpreted as H or D atoms and inserted into the refinement using fixed atomic coordinates (derived from the difference Fourier maps) and isotropic a.d.p.s. The refinement of the site occupancy factors (SOFs) of such positions invariably resulted in negative occupancy, disproving the presence of localized hydroxyl groups.

At convergence the SOFs of the *T* sites were refined in both structures to check for ordered Si vacancies. Three different refinement strategies were tested in an attempt to critically compare the results obtained under different assumptions. Since parameter correlation in such a complex refinement is

[1] Supplementary data for this paper are available from the IUCr electronic archives (Reference: NA0094). Services for accessing these data are described at the back of the journal.

unavoidable during least-squares minimization because of the large number of parameters, the adopted procedure is believed at least to indicate the presence of heavily biased results. The adopted strategies were as follows: (*a*) simultaneous refinement of the SOFs of all *T* sites, together with one isotropic atomic displacement parameter for all *T* sites; (*b*) simultaneous refinement of the SOFs of all *T* sites, keeping the isotropic a.d.p. of the *T* sites at the previously refined value; (*c*) refinement of the SOF of one *T* site at a time, together with one free isotropic a.d.p. for all *T* sites.

The results of the refinements for the MONO samples clearly indicated strong parameter correlations during the refinements: the resulting SOFs of the 24 independent *T* sites were significantly different depending on the adopted strategy and the starting parameter set. The observed data are considered not sufficient to support such a detailed refinement, and the refined SOFs are to be considered unreliable.

On the other hand the refinement of the *T* site SOFs using the ORTHO data consistently converged to similar results, independently of the assumed strategy. The SOFs of sites Si(6), Si(7), Si(10) and Si(11) systematically converged to values in the range 0.69–0.78, with mean values around 0.75 (5). The SOFs of all other tetrahedral sites refined to values in the range 0.88–1.13, *i.e.* full occupancy within 3 e.s.d.s. Such values were consistently obtained independently of the assumed atomic displacement parameters (freely refinable or fixed), of the starting parameter set and of the refinement strategy. The resulting total content of Si atoms in the ORTHO sample following the refinement (*i.e.* eight fully occupied *T* sites and four partially occupied sites at the 75% level) is 88 Si atoms per cell, which is surprisingly close to the expected value from the chemical analysis (87.36 or 88.32 Si atoms per cell assuming $x = 0.09$ or $x = 0.08$, respectively).

The refined low occupancy factors of the Si(6), Si(7), Si(10) and Si(11) tetrahedral sites are considered as

Table 3
Refined atomic coordinates of monoclinic D-silicalite (MONO sample).

$$U_{\rm eq} = (1/3)\Sigma_i\Sigma_j U^{ij} a^i a^j \mathbf{a}_i.\mathbf{a}_j.$$

The final refinement was performed with full occupancy on all Si and O atoms (see text for details). The average Si—O tetrahedral distances (Å) are reported for the *T* sites, and the Si—O—Si angles (°) are reported for the O sites.

	x	*y*	*z*	Mean Si—O distance	$U_{\rm eq}$
Si(1)	0.0622 (4)	0.4223 (4)	−0.3282 (6)	1.611 (1)	0.0114 (5)
Si(2)	0.0329 (4)	0.3195 (4)	−0.1641 (5)	1.610 (1)	0.0114 (5)
Si(3)	0.0605 (4)	0.2820 (4)	0.0600 (5)	1.609 (1)	0.0114 (5)
Si(4)	0.0628 (4)	0.1253 (4)	0.0358 (7)	1.610 (1)	0.0114 (5)
Si(5)	0.0307 (4)	0.0781 (4)	−0.1760 (6)	1.609 (1)	0.0114 (5)
Si(6)	0.0546 (4)	0.2006 (4)	−0.3115 (5)	1.610 (1)	0.0114 (5)
Si(7)	−0.1737 (4)	0.4250 (4)	−0.3190 (6)	1.610 (1)	0.0114 (5)
Si(8)	−0.1250 (4)	0.3098 (4)	−0.1726 (6)	1.609 (1)	0.0114 (5)
Si(9)	−0.1782 (4)	0.2730 (4)	0.0389 (5)	1.610 (1)	0.0114 (5)
Si(10)	−0.1777 (4)	0.1193 (5)	0.0334 (6)	1.610 (1)	0.0114 (5)
Si(11)	−0.1267 (4)	0.0715 (4)	−0.1714 (6)	1.610 (1)	0.0114 (5)
Si(12)	−0.1596 (3)	0.1897 (4)	−0.3167 (6)	1.610 (1)	0.0114 (5)
Si(13)	0.4458 (4)	0.4303 (4)	−0.3369 (6)	1.610 (1)	0.0114 (5)
Si(14)	0.4775 (4)	0.3144 (4)	−0.1889 (6)	1.609 (1)	0.0114 (5)
Si(15)	0.4395 (4)	0.2742 (4)	0.0222 (5)	1.609 (1)	0.0114 (5)
Si(16)	0.4358 (4)	0.1202 (4)	0.0417 (6)	1.609 (1)	0.0114 (5)
Si(17)	0.4739 (4)	0.0732 (5)	−0.1745 (6)	1.610 (1)	0.0114 (5)
Si(18)	0.4365 (3)	0.1871 (4)	−0.3115 (6)	1.609 (1)	0.0114 (5)
Si(19)	0.6710 (4)	0.4237 (4)	−0.3098 (6)	1.610 (1)	0.0114 (5)
Si(20)	0.6341 (4)	0.3099 (4)	−0.1709 (6)	1.609 (1)	0.0114 (5)
Si(21)	0.6646 (4)	0.2738 (4)	0.0454 (6)	1.610 (1)	0.0114 (5)
Si(22)	0.6685 (4)	0.1203 (4)	0.0347 (6)	1.610 (1)	0.0114 (5)
Si(23)	0.6333 (4)	0.0714 (4)	−0.1818 (6)	1.610 (1)	0.0114 (5)
Si(24)	0.6840 (3)	0.1956 (4)	−0.2963 (5)	1.610 (1)	0.0114 (5)

	x	*y*	*z*	Si—O—Si angle	$U_{\rm eq}$
O(1)	0.0619 (6)	0.3829 (5)	−0.2232 (8)	145.2 (8)	0.0134 (4)
O(2)	0.0636 (5)	0.3100 (7)	−0.0528 (5)	152.4 (9)	0.0134 (4)
O(3)	0.0470 (5)	0.2036 (4)	0.0447 (8)	159.0 (8)	0.0134 (4)
O(4)	0.0718 (6)	0.1068 (6)	−0.0806 (7)	141.6 (9)	0.0134 (4)
O(5)	0.0444 (6)	0.1260 (5)	−0.2700 (8)	148.1 (9)	0.0134 (4)
O(6)	0.0519 (6)	0.2500 (5)	−0.2169 (8)	152.8 (9)	0.0134 (4)
O(7)	−0.1567 (6)	0.3732 (5)	−0.2300 (8)	159.7 (9)	0.0134 (4)
O(8)	−0.1703 (5)	0.2947 (6)	−0.0763 (6)	151.6 (9)	0.0134 (4)
O(9)	−0.1555 (5)	0.1963 (4)	0.0302 (8)	147.2 (8)	0.0134 (4)
O(10)	−0.1741 (6)	0.0909 (6)	−0.0791 (7)	146.7 (9)	0.0134 (4)
O(11)	−0.1511 (6)	0.1184 (5)	−0.2627 (7)	152.6 (9)	0.0134 (4)
O(12)	−0.1264 (6)	0.2472 (5)	−0.2479 (8)	156.8 (9)	0.0134 (4)
O(13)	−0.0470 (4)	0.3236 (6)	−0.1450 (8)	154.0 (8)	0.0134 (4)
O(14)	−0.0479 (4)	0.0859 (6)	−0.1505 (9)	152.6 (9)	0.0134 (4)
O(15)	0.1359 (4)	0.4230 (5)	−0.3771 (7)	132.0 (8)	0.0134 (4)
O(16)	−0.0015 (5)	0.3862 (6)	−0.3810 (7)	155.6 (9)	0.0134 (4)
O(17)	−0.1352 (5)	0.4090 (6)	−0.4215 (7)	139.5 (9)	0.0134 (4)
O(18)	0.1308 (4)	0.2066 (6)	−0.3499 (7)	134.6 (8)	0.0134 (4)
O(19)	0.0025 (5)	0.2116 (6)	−0.4035 (7)	168.2 (9)	0.0134 (4)
O(20)	−0.1256 (4)	0.1944 (7)	−0.4251 (7)	140.0 (7)	0.0134 (4)
O(21)	0.0486 (6)	0.0036 (4)	−0.2113 (9)	138.4 (9)	0.0134 (4)
O(22)	−0.1425 (6)	−0.0026 (4)	−0.2111 (8)	149.3 (9)	0.0134 (4)
O(23)	−0.2526 (4)	0.4293 (6)	−0.3478 (8)	146.9 (9)	0.0134 (4)
O(24)	−0.2391 (3)	0.2036 (6)	−0.3310 (8)	151.6 (8)	0.0134 (4)
O(25)	−0.2560 (4)	0.2763 (6)	0.0710 (8)	151.9 (9)	0.0134 (4)
O(26)	−0.2541 (4)	0.1160 (7)	0.0721 (8)	142.8 (9)	0.0134 (4)
O(27)	0.4592 (6)	0.3852 (5)	−0.2389 (7)	150.2 (9)	0.0134 (4)
O(28)	0.4584 (5)	0.3196 (5)	−0.0725 (6)	141.6 (7)	0.0134 (4)
O(29)	0.4292 (5)	0.1957 (4)	0.0025 (8)	149.3 (8)	0.0134 (4)
O(30)	0.4461 (6)	0.0820 (6)	−0.0628 (6)	155.1 (9)	0.0134 (4)
O(31)	0.4288 (5)	0.1200 (5)	−0.2468 (8)	139.0 (8)	0.0134 (4)
O(32)	0.4405 (6)	0.2513 (5)	−0.2394 (9)	154.1 (9)	0.0134 (4)
O(33)	0.6676 (6)	0.3775 (5)	−0.2115 (7)	141.6 (8)	0.0134 (4)
O(34)	0.6418 (5)	0.3167 (5)	−0.0512 (6)	140.6 (9)	0.0134 (4)
O(35)	0.6441 (5)	0.1967 (4)	0.0315 (7)	146.9 (7)	0.0134 (4)

Table 3 (continued)

	x	y	z	Si—O—Si angle	U_{eq}
O(36)	0.6588 (6)	0.0785 (6)	−0.0673 (6)	151.8 (9)	0.0134 (4)
O(37)	0.6726 (6)	0.1212 (5)	−0.2551 (8)	149.0 (9)	0.0134 (4)
O(38)	0.6750 (6)	0.2439 (5)	−0.2013 (8)	139.2 (9)	0.0134 (4)
O(39)	0.5562 (3)	0.2969 (6)	−0.2002 (8)	150.5 (9)	0.0134 (4)
O(40)	0.5536 (4)	0.0868 (6)	−0.1830 (9)	158.6 (9)	0.0134 (4)
O(41)	0.3761 (5)	0.4211 (6)	−0.3987 (8)	154.7 (9)	0.0134 (4)
O(42)	0.5025 (5)	0.4190 (6)	−0.4199 (7)	149.6 (9)	0.0134 (4)
O(43)	0.6317 (5)	0.3909 (6)	−0.4040 (8)	150.5 (9)	0.0134 (4)
O(44)	0.3669 (4)	0.1925 (7)	−0.3744 (7)	150.1 (9)	0.0134 (4)
O(45)	0.5021 (4)	0.1801 (5)	−0.3802 (6)	146.8 (8)	0.0134 (4)
O(46)	0.6346 (5)	0.2119 (6)	−0.3899 (7)	151.5 (8)	0.0134 (4)
O(47)	0.4625 (6)	−0.0041 (5)	−0.2021 (8)	150.3 (9)	0.0134 (4)
O(48)	0.6448 (6)	−0.0041 (4)	−0.2182 (9)	142.4 (9)	0.0134 (4)

possible evidence of long-range ordering of Si vacancies, and therefore the difference Fourier maps around these sites were thoroughly checked for possible evidence of H atoms. No significant peaks were found at a meaningful distance from the involved framework O atoms. The structure refinement therefore indicates that the H atoms of the hydroxyl groups must be disordered on multiple configurations. If we take into account that the Si $\rightarrow$ 4OH coupled substitution is involved, and that the OH groups are distributed on the four tetrahedral O atom sites, then we have a 25% probability of locating an H atom in the proximity of each O atom site. Moreover, assuming that the OH group is positioned within the framework tetrahedron with the H atom slightly displaced from the tetrahedral O—O edge (as in the hydrogarnet configuration; Lager & Von Dreele, 1996), then each H atom can be statistically disordered on six alternative positions, each site having a 4.2% occupancy probability. If we assume that the H atoms can also be located at positions outside the framework tetrahedron, then the statistical occupancy is even lower. Such low occupancy positions are hardly to be detected in the difference Fourier maps.

The fact that three out of the four observed defective *T* sites are adjacent to each other [Si(7)—O(35)—Si(7), Si(7)—O(34)—Si(11), Si(10)—O(22)—Si(11), Si(10)—O(38)—Si(10)] implies that, in principle, vacancy clusters up to six Si defects are possible [*i.e.* Si(7)—Si(7)—Si(11)—Si(10)—Si(10)—Si(11) loop]. This is in agreement with the model of hydroxyl nests in silicalite put forward on the basis of spectroscopic evidence (Zecchina, Bordiga, Spoto, Marchese, Petrini, Leofanti & Padovan, 1992; Zecchina, Bordiga, Spoto, Scarano *et al.*, 1992; Zecchina, Bordiga, Spoto, Marchese, Petrini, Leofanti, Padovan & Otero Areàn, 1992; Bordiga, Ricchiardi *et al.*, 1994; Marra *et al.*, 1994). Of course, the presence of clusters of Si vacancies makes the geometrical and crystal-chemical interpretation of the OH clusters more complicated, and justifies the random distribution of H atoms suggested by the diffraction results. This observation is particularly relevant since it can explain two independent experimental evidences: (i) the increased adsorption properties of defective silicalites, not accounted for by isolated *T* vacancies (Zecchina, Bordiga, Spoto, Marchese, Petrini, Leofanti & Padovan, 1992), and (ii) the presence of an IR absorption band in the skeleton stretching mode region at about 900 cm^{-1}. This band was previously ascribed to distorted Si—O—Si bridges (Zecchina, Bordiga, Spoto, Scarano *et al.*, 1992) and successively attributed to a double oxygen bridge between two adjacent Si atoms located in the proximity of a hydroxyl nest, on the basis of a combined IR and *ab initio* study (Pelmenschikov *et al.*, 1993). As a matter of fact, the elimination of two adjacent Si(10) atoms makes the formation of a double oxygen bridge between two adjacent Si(9) atoms possible, and the elimination of two adjacent Si(11) atoms makes the formation of three double links possible, *i.e.* between two adjacent Si(7) atoms, two adjacent Si(12) atoms, or two adjacent Si(10) atoms.

Furthermore, molecular mechanics simulations (Marra *et al.*, 1994) have shown that the equilibrium positions of internal OH groups is critically dependent on the properties of the assumed nest. Due to the strong interaction between OH groups *via* hydrogen bonds, the equilibrium position of each given H atom is heavily perturbed by the configuration of the nearby OH groups substituting a vacant *T* site. For example, there is one nest configuration generated by the simultaneous vacancy of all six *T*-site [Fig. 1*b*; two Si(7), two Si(10) and two Si(11)], six nest configurations based on five *T*-site vacancies, and 15 nest configurations based on *T*-site vacancy couples. Each configuration shows a specific set of equilibrium positions of the hydroxyl population in the MFI unit cell. Of course, the random presence of several among the possible nest configurations determines a spread in the H-atom location, whereas it additively contributes to the reduction of the Si-atom SOFs. The case of Si(6) is different as it is isolated from the Si(7), Si(10), Si(11) site cluster and also from neighbouring Si(6) sites. It is also worth noting that the molecular mechanics simulations of several nest configurations show the presence of multiple local minima for the H atom of an OH group, and that the low potential barriers between alternative sites might be easily overcome even at room temperature.

The suggestion inferred from the molecular mechanics simulations is that the H (or D) atoms in MFI could in principle be located from the diffraction analysis only if one specific nest configuration is energetically favoured, *i.e.* if the same *T* sites are simultaneously missing in all the defective unit cells. The failure of locating the H (or D) atoms is a strong indication that several of the possible nest configurations are present simultaneously. The interpretation is in agreement with the information derived from IR spectroscopy, since the presence of a broad band in the 3600–2800 cm^{-1} range indicates a heterogeneous

distribution of OH═OH distances (Zecchina, Bordiga, Spoto, Marchese, Petrini, Leofanti & Padovan, 1992; Zecchina, Bordiga, Spoto, Scarano *et al.*, 1992; Zecchina, Bordiga, Spoto, Marchese, Petrini, Leofanti, Padovan & Otero Areàn, 1992; Bordiga, Ricchiardi *et al.*, 1994; Marra *et al.*, 1994).

4. Conclusions

The present work presents the first neutron diffraction study performed on MFI-type structures. The essential features of both orthorhombic and monoclinic silicalite frameworks as described in the literature (Van Koningsveld *et al.*, 1987, 1990) are confirmed, including the mild correlation between Si—O distances and Si—O—Si angles.

Furthermore, the availability of high-resolution neutron diffraction data allowed testing of the ordered distribution of Si vacancies in the tetrahedral framework. In monoclinic silicalite no evidence was found of long-range order in the Si vacancies, whereas they are ordered on four tetrahedral sites [Si(6), Si(7), Si(10) and Si(11)] in orthorhombic silicalite. The low occupancy of the proton sites precluded location of the OH groups, which are assumed to be randomly distributed on the tetrahedral oxygen sites related to the defective Si sites. The totally random distribution of Si vacancies (and OH groups) observed in monoclinic deuterated silicalite may be ascribed to the distribution of defects over a larger number of framework sites (24 independent tetrahedral atoms), due to a higher flexibility of the structure, but could also be due to the partial diffusion and randomization of the defects during the deuteration process.

The SERC is acknowledged for neutron beam time at ISIS. The experiment (RB 8702) was partially supported by a grant under the CNR-SERC agreement. General financial support was provided by the Italian CNR and MURST through research grants to GA. R. Ibberson kindly helped with data collection. A. Zecchina, S. Bordiga, G. Petrini, F. Rivetti are acknowledged for fruitful discussions. R. Buzzoni and G. Spanò synthesized and deuterated the samples. CL acknowledges the financial support of the MURST (Cofin 98, Area 03) project coordinated by A. Zecchina.

References

Bayese, C. R., Kentgens, A. P. R., de Haan, J. W., van de Ven, L. J. M. & van Hooff, J. H. C. (1992). *J. Phys. Chem.* **96**, 755–782.
Bolis, V., Bordiga, S., Lamberti, C., Zecchina, A., Carati, A., Petrini, G., Rivetti, F. & Spanò, G. (1999*a*). *Microporous Mesoporous Mater.* **30**, 67–76.
Bolis, V., Bordiga, S., Lamberti, C., Zecchina, A., Carati, A., Petrini, G., Rivetti, F. & Spanò, G. (1999*b*). *Langmuir*, **15**, 5753–5764.
Bordiga, S., Buzzoni, R., Geobaldo, F., Lamberti, C., Giamello, E., Zecchina, A., Leofanti, G., Petrini, G., Tozzola, G. & Vlaic, G. (1996). *J. Catal.* **158**, 486–501.
Bordiga, S., Coluccia, S., Lamberti, C., Marchese, L., Zecchina, A., Boscherini, F., Buffa, F., Genoni, F., Leofanti, G., Petrini, G. & Vlaic, G. (1994). *J. Phys. Chem.* **98**, 4125–4132.
Bordiga, S., Ricchiardi, G., Lamberti, C., Scarano, D., Spoto, G. & Zecchina, A. (1994). *Mater. Eng.* **5**, 197–209.
Chu, C. T.-W. & Chang, C. (1985). *J. Phys. Chem.* **89**, 1569–1571.
Coudurier, G., Auroux, A., Vedrine, J. C., Farlee, R. D., Abrams, L. & Shannon, R. D. (1987). *J. Catal.* **108**, 1–14.
Dessau, R. M., Schmitt, K. D., Kerr, G. T., Woorely, G. L. & Alemany, L. B. (1987). *J. Catal.* **104**, 484–489.
Flaningen, E. M., Bennett, J. M., Grose, R. W., Cohen, J. P., Patton, R. L., Kirchner, R. & Smith, J. V. (1978). *Nature (London)*, **271**, 512–514.
Geobaldo, F., Lamberti, C., Bordiga, S., Zecchina, A., Turnes Palomino, G. & Otero Areán, C. (1996). *Catal. Lett.* **42**, 25–33.
Hunger, M., Herger, J., Pfeifer, H., Caro, J., Zibrowius, B. & Mostowicz, R. (1987). *J. Chem. Soc. Faraday Trans. I*, **83**, 3459.
Ikeda, S. & Carpenter, J. M. (1985). *Nucl. Instrum. Methods Phys. Res. A*, **239**, 536–544.
Kokotailo, G. T., Lawton, S. L., Olson, G. T. & Meier, W. M. (1978). *Nature (London)*, **272**, 437–439.
Lager, G. A. & Von Dreele, R. B. (1996). *Am. Miner.* **81**, 1097–1104.
Lamberti, C., Bordiga, S., Arduino, D., Zecchina, A., Geobaldo, F., Spanò, G., Genoni, F., Petrini, G., Carati, A., Villain, F. & Vlaic, G. (1998). *J. Phys. Chem. B*, **102,** 6382–6390.
Lamberti, C., Bordiga, S., Zecchina, A., Carati, A., Fitch, A. N., Artioli, G., Petrini, G., Salvalaggio, M. & Marra, G. L. (1999). *J. Catal.* **183**, 222–231.
Larson, A. C. & Von Dreele, R. B. (1998). *GSAS General Structure Analysis System.* Document LAUR 86–748. Los Alamos National Laboratory, USA.
Le Noc, L., Trong On, D., Solomykina, S., Echchahed, B., Boland, F., Cartier dit Moulin, C. & Bonneviot, L. (1996). *Stud. Surf. Sci. Catal.* **101**, 611–620.
Liu, X. & Klinowski, J. (1992). *J. Phys. Chem.* **96**, 3403–3408.
Marra, G., Tozzola, G., Leofanti, G., Padovan, M., Petrini, G., Genoni, F., Venturelli, B., Zecchina, A., Bordiga, S. & Ricchiardi, G. (1994). *Stud. Surf. Sci. Catal.* **84**, 559–566.
Meier, W. M., Olson, D. H. & Baerlocher, Ch. (1996). *Atlas of Zeolite Structure Types*, 4th ed. (revised). London: Elsevier.
Millini, R., Previde Massara, E., Perego, G. & Bellussi, G. (1992). *J. Catal.* **137**, 497–503.
Millini, R., Perego, G. & Bellussi, G. (1999). *Top. Catal.* **9**, 13–34.
Olson, G. T., Kokotailo, G. T., Lawton, S. L. & Meier, W. M. (1981). *J. Phys. Chem.* **85**, 2238–2243.
Otero Areán, C., Turnes Palomino, G., Geobaldo, F. & Zecchina, A. (1996). *J. Phys. Chem.* **100**, 6678–6690.
Pelmenschikov, A. G., Morosi, G., Gamba, A., Zecchina, A., Bordiga, S. & Paukshtis, E. A. (1993). *J. Phys. Chem.* **97**, 11979–11986.
Scarano, D., Zecchina, A., Bordiga, S., Geobaldo, F., Spoto, G., Petrini, G., Leofanti, G., Padovan, M. & Tozzola, G. (1993). *J. Chem. Soc. Faraday Trans.* **89**, 4123–4130.
Szostak, R. M. (1989). *Molecular Sieves.* New York: Van Nostrand Reinhold.
Szostak, R. M. & Thomas, T. L. (1986). *J. Catal.* **100**, 555–557.
Taramasso, M., Perego, G. & Notari, B. (1983). US Patent No. 4410501.
Tozzola, G., Mantegazza, M. A., Ranghino, G., Petrini, G., Bordiga, S., Ricchiardi, G., Lamberti, C., Zulian, R. & Zecchina, A. (1998). *J. Catal.* **179**, 64–71.
Van Koningsveld, H., Jansen, J. C. & Van Bekkum, H. (1990). *Zeolites*, **10**, 235–242.
Van Koningsveld, H., Van Bekkum, H. & Jansen, J. C. (1987). *Acta Cryst.* B**43**, 127–132.
Vedrine, J. C., Auroux, A., Bolis, V., Dejaiifve, P., Naccache, P., Wierrzchowskii, C., Derouane, E. G., Nagy, J. B., Gilsonn, J.-P., van Hooff, J. H. C., van den Berg, J. P. & Wolthuizen, J. (1979). *J. Catal.* **59**, 248–262.

Vezzalini, G., Quartieri, S., Galli, E., Alberti, A., Cruciani, G. & Kvick, Å. (1997). *Zeolites*, **19**, 323–325.
Zecchina, A., Bordiga, S., Scarano, D., Ricchiardi, G., Lamberti, C., Petrini, G., Leofanti, G. & Mantegazza, M. (1996). *Catal. Today*, **32**, 97–106.
Zecchina, A., Bordiga, S., Spoto, G., Marchese, L., Petrini, G., Leofanti, G. & Padovan, M. (1992). *J. Phys. Chem.* **96**, 4985–4990.
Zecchina, A., Bordiga, S., Spoto, G., Marchese, L., Petrini, G., Leofanti, G., Padovan, M. & Otero Areàn, C. (1992). *J. Chem. Soc. Faraday Trans.* **88**, 2959–2969.
Zecchina, A., Bordiga, S., Spoto, G., Scarano, D., Petrini, G., Leofanti, G. & Padovan, M. (1992). *J. Phys. Chem.* **96**, 4991–4997.
Zecchina, A., Spoto, G., Bordiga, S., Padovan, M., Leofanti, G. & Petrini, G. (1991). *Stud. Surf. Sci. Catal.* **65**, 671–680.